TITLE: Mapping structure and rheology of pH-responsive resins for low-VOC coatings.

AUTHOR NAMES:

*Kush J. Patel[1], Steven Bowles[2], L. Elise Matolyak[2], Douglas Vogus[2], Chao Wang[2], Gergely Nagy[3], Jeffrey J. Richards[1]**

AUTHOR ADDRESS

1. Department of Chemical and Biological Engineering, Northwestern University, Evanston, IL, USA. 2. PPG Industries, Allison Park, PA, USA. 3. Neutron Scattering Division, Oak Ridge National Laboratory, Oak Ridge, TN, USA

KEYWORDS: Coatings, Volatile Organic Compounds, Rheology, Small Angle Scattering

ABSTRACT

In recent years, the paint and coatings industry has shifted away from traditional resin formulations which require high concentrations of volatile organic compounds (VOCs) to achieve the desired rheological performance and sustainability targets. One approach to eliminate or reduce VOCs in paint and coating formulations while maintaining the final performance is to disperse stimuli-responsive polymer latex particles in water. The chemistry and architecture of these particles have been engineered such that the suspension rheology changes in response to pH changes. The

particles can also be swollen with organic solvent to illicit similar rheological changes. To understand how the particle microstructure influences the observed macroscopic properties, we use small-angle neutron scattering (SANS) and dynamic light scattering (DLS) to determine that these particles consist of a crosslinked core with long, polymer tails that extend into the dispersing medium. Carboxylic acid groups present on the tails deprotonate with increasing pH and the extension of the polymer chain due to charge repulsion increases the hydrodynamic drag on the particle. We find that adjusting the pH alone has a much more significant effect on the shear-dependence of the viscosity of the studied resin than adding organic solvent alone. We also find that this resin architecture is more responsive per mole of pH-responsive group than other architectures of pH-responsive latex particles in literature.

SYNOPSIS

Waterborne formulations have been developed to reduce the volatile organic compound content in paints and coatings. This study links the microstructure of the engineered particles to their performance.

TEXT

Introduction:

A key market driver in many industries is to reduce environmental impact without negatively impacting product performance. One particular concern for the coatings industry is the release of volatile organic compounds (VOCs). As defined by the EPA, VOCs are organic compounds which "evaporate under normal indoor atmospheric conditions of temperature and pressure"[1]. VOCs contribute to ozone formation and negatively impact human health through their long-term climate

impacts and through acute exposure. Over the past decades, there has been significant progress in reducing VOC content in solvent-borne coatings by increasing solids content or by transitioning technologies to waterborne coatings[2,3]. While many existing waterborne technologies contain reduced VOC levels compared to similar solvent-borne coatings, they still contain significant levels of organic solvents[4,5].

Eliminating VOCs from waterborne coatings entirely remains a challenge because solvents enable key coating requirements including storage stability, application robustness, and film coalescence[6,7]. It is particularly challenging to reduce VOCs in industrial, spray-applied waterborne coatings. Formulations for spray applications must have very specific rheological properties, including a low viscosity when subjected to flow for effective atomization and a high viscosity after application to prevent sag and allow for proper film coalescence[8]. This rheological response is present when the formulation is thickened through the addition of solvent or pH resulting in a strongly shear thinning behavior. To elicit this strong-shear thinning, the chemistry and architecture of latex particles within the formulation must be engineered to respond to different chemical environments. Particles of varying architectures, including single-phase, raspberry-like, snowman-like, moon-like, or core-shell, have been explored in how they respond to stimuli, such as temperature, pH, and solvent[9–11].

The link between particle architecture and rheological response has often been studied using small angle scattering (SAS)[12,13]. By comparing the changes in structure and interactions of particles when stimuli are introduced, the mechanism of how these particles respond can be determined. For instance, the mechanism of solvent-response in polymer latex resins is often attributed to a small-molecule solvent or monomer species migrating into the particle, which thus swells the particle and expands its occupied volume[14,15]. For resins that are responsive to pH, the mechanism

is often driven by protonation or deprotonation of the pH-responsive groups as pH is adjusted. This can cause counterion migration into the particle, expanding the occupied volume due to osmotic pressure changes, as well as intra- and interparticle charge repulsion[11,15]. Additionally, telechelic polymers, which are often used as rheological modifiers in waterborne resins, can induce complex interactions between particles[16]. Repulsive interactions arise when both polymer ends attach to the same particle, forming loops, and attractive interactions arise when the polymer bridges between particles[17]. The expansion of the particle volume will appear in the particle form factor in SAS measurements, and changes in the interaction potential will appear in the interparticle structure factor. SAS is therefore a powerful tool for studying responsive materials.

We use SAS techniques to determine the architecture of a two-phase core-shell pH-responsive polymer latex particle that has been developed for low-VOC paints and coatings formulations. The formulation chosen serves as a model system for a class of similar resins used for decorative coatings. The particles consist of a crosslinked acrylic core which swells with added organic solvent and a shell layer that contains carboxylic acid groups which responds to changes in pH. The measurements reported here show that the shell layer consists of long, polymer tails which extend far from the acrylic core, imparting additional hydrodynamic drag to the core when the tails are fully extended. We compare the rheological response of the shear-dependent viscosity of this resin upon an increase in pH to its response to added organic solvent. Additionally, we compare the rheological response of other pH-responsive latex emulsions with different particle chemistries and architectures[18–20]. We find that the long, polymer tails efficiently elicit strong shear thinning while utilizing fewer pH-responsive functional groups per mass of particle.

Materials and Methods:

Synthesis: A core-shell (CS) acrylic latex resin was synthesized via a two-step emulsion polymerization using the initiator ammonium persulfate at 85 °C with a seed stage followed by two separate emulsified monomers feeds described in a patent[21]. The first monomer feed (core) consisted of a pre-emulsion of Rhodapex AB/20, methyl methacrylate, butyl acrylate, acrylamide solution, ethylene glycol dimethacrylate, and hydroxyethyl methacrylate added to the flask over 3 hours with initiator. The second monomer feed (shell) was formed by adding a pre-emulsion of Rhodapex AB/20, butyl acrylate, methacrylic acid, methyl methacrylate, and hydroxyethyl acrylate over 1.5 hours with the initiator mixture of initiator and borax. The final mixture was held for 2 hours at temperature before partial amination and addition of a biocide. The control core-only (CO) acrylic latex resin was synthesized following the same procedure and composition, polymerizing the core pre-emulsion monomer feed.

Sample preparation: The stock CS and CO resins are 24.6 w% and 23.0 w% of solid particles, respectively, dispersed in water. The pH and conductivity of the stock and prepared samples were measured using an Oakton PC 700 probe. The pH and conductivity of both stock resins was approximately 6.2 and 1230 μS/cm, respectively. The pH and ionic strength of samples were controlled using solutions of potassium hydroxide, KOH (ACS reagent, pellets, Sigma-Aldrich) and potassium chloride, KCl (ACS reagent, Fisher Chemical). Samples are diluted with 8.8 mM KCl to keep the ionic conductivity constant upon dilution. Samples with 1-butanol (ACS reagent, Sigma-Aldrich) were prepared by adding up to 1.5 grams butanol per gram of solid particle in the diluted resin. These samples were mixed using a Fisher Brand roll mixer for at least 12 hours

and left to sit to observe any potential phase separation between the aqueous phase and butanol. Very dilute samples, <5 w% particles, and samples with high amounts of butanol, ~1.5 g/g particle, were observed to phase separate. These samples were not studied further.

Rheology: Steady shear flow curves were measured using a TA Instruments DHR-2 rheometer equipped with a 40 mm diameter, 2° cone with a Peltier plate. The temperature of the sample was maintained by the Peltier plate at 25 °C. A solvent trap was used to prevent excessive solvent evaporation during the measurements. Each sample underwent a pre-shear conditioning step where a constant shear rate of 100 s^{-1} was applied for 60 seconds. This pre-shear step was followed by a flow sweep from 1 s^{-1} to 1000 s^{-1} to obtain the shear rate dependent viscosity. The viscosity at shear rates greater than 10 s^{-1} was averaged using the built-in 'steady state sensing' function on the TRIOS software where an average was taken over a 10 second sample period and the point was accepted if it was the third consecutive point to be within a 5% difference from the previous sample period. For shear rates below 10 s^{-1}, the sample was allowed to equilibrate for 15 seconds followed by a 90 second averaging period so that rotational differences of the rheometer and geometry can be averaged out. The viscosity measured by the rheometer is normalized to the viscosity of water to obtain the relative viscosity, $\eta_r = \eta/\eta_s$.

Small-angle Neutron Scattering (SANS): Measurements were performed at the EQ-SANS beamline[22] at the Spallation Neutron Source at Oak Ridge National Laboratory (Oak Ridge, TN). Samples were prepared as described above. We prepared dilute samples using deuterium oxide, D_2O (99.9 atom % D, Sigma-Aldrich) to achieve a solvent weight ratio of D_2O to H_2O of 0.96. Concentrated samples are prepared in H_2O only. The two instrument configurations used were as follows: a neutron wavelength band of 15 Å – 17.9 Å with a sample to detector distance of 9 m covering a momentum transfer range from 0.002 to 0.034 $Å^{-1}$, and a neutron wavelength band of

4 Å – 7.6 Å with a sample to detector distance of 4 m covering a momentum transfer range from 0.009 to 0.282 $Å^{-1}$. Data reduction was performed with the help of the drtsans software[23]. Scattering intensities were corrected for background (empty cell) scattering, sample transmission, and detector sensitivity resulting in scattering intensities in absolute scale. The corrected 2-D detector images were then circularly averaged to obtain the scattering intensity, I, vs wavevector, Q, and the two instrument configurations were merged to obtain measurements over the total accessible Q-range.

Dynamic Light Scattering and Zetapotential: Measurements were taken using a Malvern Zetasizer Ultra at Northwestern University Atomic and Nanoscale Characterization Experimental Center. The resins were diluted to 0.05 w% and loaded into Malvern DTS1070 cells. The diffusion coefficient of the particle is determined using a cumulants fit to the electric field autocorrelation function. The surface charge density is calculated from the measured electrophoretic mobility using methods described in Makino and Ohshima[24].

Results and Discussion:

Chemistry of the resins

Core-shell (CS) particles were synthesized following a procedure described in a patent[21]. Briefly, this involves a two-step emulsion polymerization in which radical-initiated polymerization occurs in surfactant micelles to produce spherical particles. In the first stage, several acrylic monomers (methyl methacrylate, butyl acrylate, acrylamide solution, and hydroxyethyl methacrylate) were cross-linked with ethylene glycol dimethacrylate, to form the core of the particle. The shell was polymerized to the core by adding acrylic monomers (butyl acrylate, methacrylic acid (MAA), methyl methacrylate, and hydroxyethyl acrylate) with no cross-linking

agent. The MAA in the shell is pH responsive and deprotonates upon an increase in pH. Core-only (CO) particles are also synthesized by stopping the synthesis after the core monomer addition. In Figure 1, the relative zero-shear viscosities, $\eta_{r,0} = \eta_0/\eta_s$, of the CS and CO resins at 10 w% solids are plotted for different stimuli conditions. Without any stimuli, at pH 6, the CS resin shows a higher viscosity than the CO resin due to the increase in the effective volume fraction of the particles when the shell is present. Upon addition of butanol, the viscosity increases for both CS and CO resins. While not shown here, other alcohols also increase the viscosity of both particles to a lesser extent (Figure S1). We hypothesize that butanol partitions into the core of the particles, swelling the particles and thus increases the effective volume fraction and relative viscosity.[25] The increase in relative viscosity with addition of butanol aligns well with literature reporting a variety of types of solvent-swellable polyacrylic latex particles[14,15]. Increasing the pH of the resins to 9, the CS resin viscosity increases dramatically whereas the CO resin viscosity remains constant. MAA, only present in the shell, contains carboxylic acid groups which deprotonate upon an increase in pH.

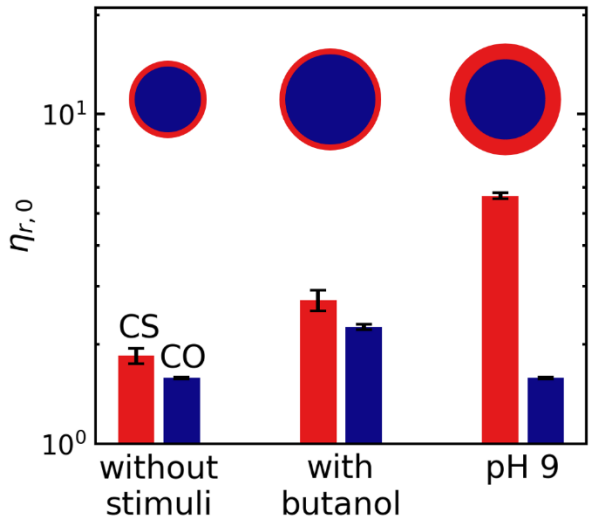

Figure 1: Relative zero-shear viscosity of CS and CO resins at 10 w% for different stimuli conditions. The viscosity increases for both resins with added butanol as the core swells and increases the effective volume fraction of the particles. Only the CS resin responds to an increase in pH as the carboxylic acid groups which give rise to the pH-responsive behavior are only present in the shell.

Previous studies on similar pH-responsive latex resins attribute the increase in viscosity with pH to the electrostatic repulsion which drives extension of the shell polymer as a result of the increase in charge in the shell or an increase in osmotic pressure due to counterion migration.[11] The degree of response will depend on the molar ratio of acid groups, crosslink density, and architecture of the particles among other factors. For this resin, the mass ratio of the shell to the core is approximately 18:82. There are approximately 2.64×10^{-3} moles of MAA per gram of shell or 3.39×10^{-4} moles of MAA per gram of particle. Comparatively, this is fewer moles of pH-responsive group (acid or base) per gram of particle than other resins reported in literature[18–20]. Further, the shell in this resin is not crosslinked, differentiating this resin architecture from some others seen in literature.

Determining the particle architecture

In Figure 2, we used SANS to measure the form factor of the CS resin at pH 6 and 9 and of the CO resin. The form factor is measured in the dilute limit of particle concentration to isolate individual particle shape and size. We were unable to measure the form factor with added butanol because in the dilute regime where the form factor is measured, butanol phase separated from the aqueous phase rather than partitioning into the particles. In the low-Q limit, we can calculate the radius of gyration of the particles using the Guinier method[26]. Here we see that the

scattering profiles of the CS resin at both low and high pH are similar to that of the CO scattering and give nearly identical $R_g \approx 51$ nm. The core of the particle is therefore primarily dominating the scattering at low Q.

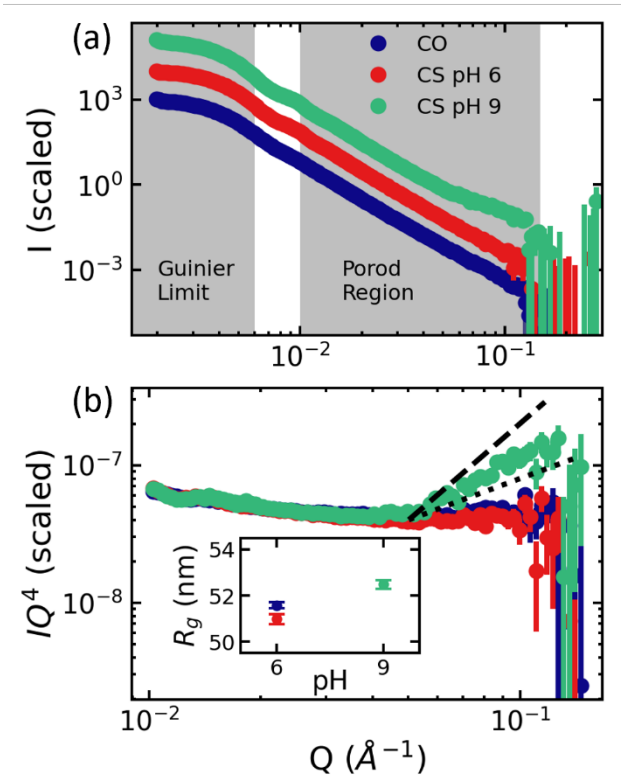

Figure 2: (a) Small-angle neutron scattering form factor of CO resin at pH 6 (blue) and CS resin at pH 6 (red) and pH 9 (green). The intensity is scaled for clarity. (b) The Porod Region is plotted as IQ^4 vs Q to highlight the Q^{-4} scaling in this region for both the CS and CO resins at pH 6. At $Q' \approx 5.6 \times 10^{-2}$ Å^{-1}, the slope of the high pH CS scattering changes. Slopes corresponding to collapsed polymer chains (dotted) and fully swollen polymer chains (dashed) are shown for comparison. The radius of gyration is calculated using the Guinier Limit (shaded region at low Q) and plotted as a function of pH in the inset of (b).

At high Q, we observe a change in the form factor for the CS particles at pH 9 at $Q' \approx 5.6 \times 10^{-2}$ Å^{-1}, where Q′ is the approximate value at which the slope of the intensity decay changes. This Q-value corresponds to a length scale of $\frac{2\pi}{Q'} \approx 11$ nm. This is in the Porod region of the scattering profile where the local structure and surface interfaces are probed[27]. The intensity in the Porod region scales as $I \propto Q^{-n}$, where the power law exponent, n, reveals information about the local structure. A power law of $n = 4$ corresponds to a smooth surface between the particle and the solvent phase which is the case for all three samples plotted in Figure 2 below Q′. In Figure 2b, the data in the Porod region is replotted as IQ^4 vs Q. For the CS resin at pH 9, the upturn at high-Q is indicative of the extended shell polymer. Fully swollen and collapsed chains will have a high-Q slope of $n = 1.6$ or 3, respectively. The bounds of this power law scaling are represented in Figure 2b as the dashed and dotted lines, respectively. The value of n for the pH 9 CS resin for $Q > Q'$ is 2.5, consistent with partially swollen chains. Neither the pH 6 CO resin nor the pH 6 CS resins show this feature, therefore the core scattering dominates the signal intensity at all length scales at low pH conditions. This indicates that the shell component, rather than a dense, crosslinked layer, consists of long polymer chains that can collapse and swell upon changes in pH. At low pH, these chains collapse, and the scattering profile is dominated by the cores. Upon an increase in pH, the carboxylic acid groups on the chains are deprotonated and the chains swell likely due to charge repulsion. The scattering contribution of the swollen shell is now commensurate with that of the core at high Q. SANS measurements support the idea that the structure of the particles is core with long, polymer tails.

The fact that the shell polymer forms long polymer chains is further supported by measurements of the particle diffusivity and surface charge density in the dilute limit. In Figure 3a, the diffusion coefficient of the particles, as determined from DLS measurements, is plotted as a function of pH

for both the CS and CO resins. The bare cores are unaffected by pH changes, whereas the diffusivity of the CS resin is decreased. By the Stokes-Einstein equation for spherical particles, the diffusivity, D, given as $\frac{k_B T}{6\pi\eta_s R_h}$, can decrease either due to an increase in the hydrodynamic size, R_h, of the particle or due an increase in η_s at fixed temperature. We considered the case that the shell component was detached from the cores and a change in conformation of a potentially dissolved polymer species would thus correspond to the observed change in solvent viscosity. However, this was ruled out because the required change in solvent viscosity to align with DLS measurements was greater than the actual measured change on the rheometer (Figure S2a). Additionally, a third resin was synthesized in which the attachment of the shell component to the cores was strictly inhibited. This resin was not shelf stable and formed an irreversible, solid mass in its stock container (Figure S2b) and thus does not share the same architecture of the CS resin.

While the shell component must therefore be attached to the cores, the pH responsive component is not present near the surface of the cores. In Figure 3b, the surface charge density of the CS and CO particles are plotted as a function of pH. The surface charge measured is the same for the CS particle as the bare core across all pH values tested. The pH response arises from the deprotonation of the carboxylic acid groups in the shell component and therefore, should result in an increase in negative charge. Because this increase is absence in our measurements, the shell component must therefore be a long, polymer chain which is tethered to the core but extends far into the solvent phase. This is also a necessary requirement for the radius of gyration, determined from the SANS measurements, to not be sensitive to the presence of the swollen shell polymer.

The diffusion of this type of particle consisting of spherical cores with tethered polymer chains was described by Ge and Rubinstein[28]. The diffusion coefficient is related to the coefficient of

friction, ζ, of the particle by the Stokes-Einstein equation, $D = \frac{k_B T}{\zeta} = \frac{k_B T}{\zeta_{core} + \zeta_{chain}}$. For these particles, in the limit of single tethered chains, the coefficient of friction is a linear combination of that of the bare particles and that of the tethered chain. When the radius of gyration of the polymer chain is much smaller than the diameter of the core, $R_{chain} \ll d_{core}$, the friction is dominated by the contribution due to the core and thus $\zeta \approx \zeta_{core}$ and $D \approx D_{core}$. This limit is seen in Figure 3a where the diffusion coefficient of the CS particle at pH 6 is approximately the same as the diffusion coefficient of the CO particle. Upon increasing pH, the chains undergo a conformation change due charge repulsion between the deprotonated carboxylic acid groups and the contribution to the friction coefficient becomes relevant.

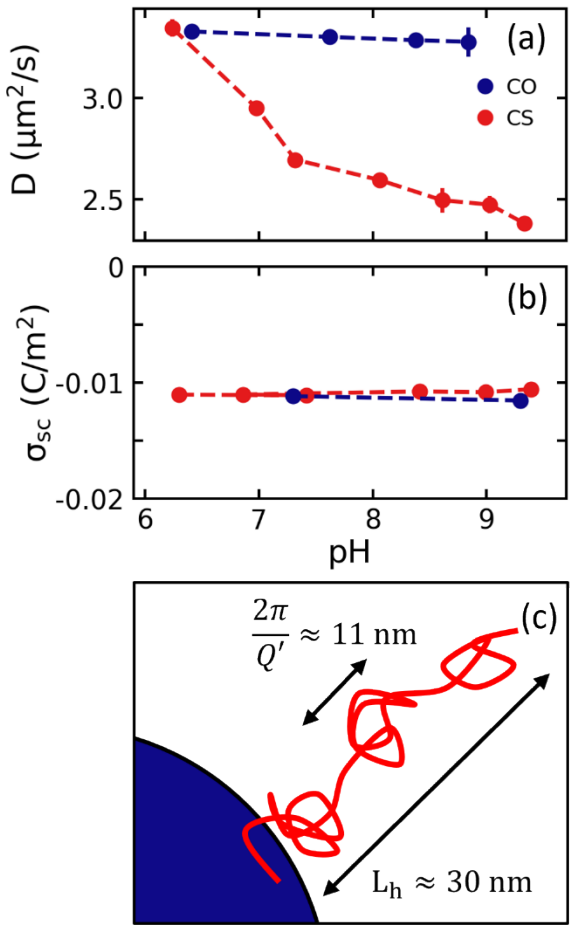

Figure 3: (a) Diffusion coefficient and (b) surface charge density of CO and CS particles as a function of pH in dilute conditions. (c) Depiction of chain hydrodynamic length, L_H, as determined by DLS compared to the length scale acquired from SANS

We calculate the hydrodynamic radius of the core, $R_{h,\,core} \approx 80$ nm, using the Stokes-Einstein equation. Similarly, the total effective hydrodynamic radius of the CS particle can be calculated. At pH 9, this is $R_{h,CS} \approx 110$ nm. Given that $\zeta_{CS} = \zeta_{core} + \zeta_{chain}$, it follows that $R_{h,CS} = R_{h,core} + L_{h,chain}$, where $L_{h,chain} \approx 30$ nm is the effective hydrodynamic length of the chain. As represented in Figure 3c, L_h is the length of the chain required to achieve the observed change in the particle diffusion. This differs from the length scale identified in the SANS form factor, $\frac{2\pi}{Q'} = 11$ nm, where the SANS length scale likely represents internal correlations between segments on the polymer chains. It is difficult to definitively assign the SANS length scale to a feature on the chain as the form factor is convoluted with the core scattering. Despite this, we are able to draw insights from SANS and DLS to formulate an understanding of the particle architecture.

Structural and Rheological Response to Stimuli

While the shell component is responsive to increases in pH, the CS resin also responds to added organic solvents, such as butanol. This is a traditional response seen in latex resins as the organic solvent partitions into the cores and swells the particles. To compare the effect of pH stimuli and organic solvent stimuli, the scattering of the CS resin is plotted in Figure 4 as a function of concentration at pH 6, with butanol (top), and at pH 9, without butanol (bottom). Butanol is

added in a 1:1 ratio with the particle weight fraction for consistency. These curves are normalized such that the Porod region at high Q overlaps. Traditionally, for small-angle scattering, the structure factor of the sample can be obtained by normalizing the intensity by the form factor since $I(Q) \propto P(Q)S(Q;\phi)$. However, in this case the particle form factor may not be constant with concentration as the degree of swelling of the particles may be a function of concentration. We can instead normalize the scattering intensity by the form factor of the cores to obtain an effective structure factor that we define here as $S'(Q) = \frac{I(Q)}{P_{core}(Q)}$. Plotting $S'(Q)$ for small Q, we can make some qualitative observations on the difference between the two stimuli studied. We see that for the high pH samples, the intensity at $Q \rightarrow 0$ is diminished at higher concentrations which is not seen in the samples with butanol. This diminishment at low Q is indicative of repulsive interactions between particles. There is an enhanced electrostatic repulsion between the particles as the carboxylic acid groups become deprotonated upon an increase in pH. In contrast, the key feature for the butanol samples is the primary peak of $S'(Q)$ at $Q \approx 3.7 \times 10^{-3}$ Å^{-1} corresponding to a length scale of ≈ 170 nm. For hard spheres, the position of this peak corresponds to the effective hard sphere diameter. The peak shifts to lower Q as we increase the concentration of particles corresponding to a larger effective diameter. The amount of solvent imbued by the particles is dependent, therefore, on the concentration of particles as well as the concentration of organic solvent indicating that some equilibrium is achieved for the organic solvent between the particle phase and the bulk aqueous phase.

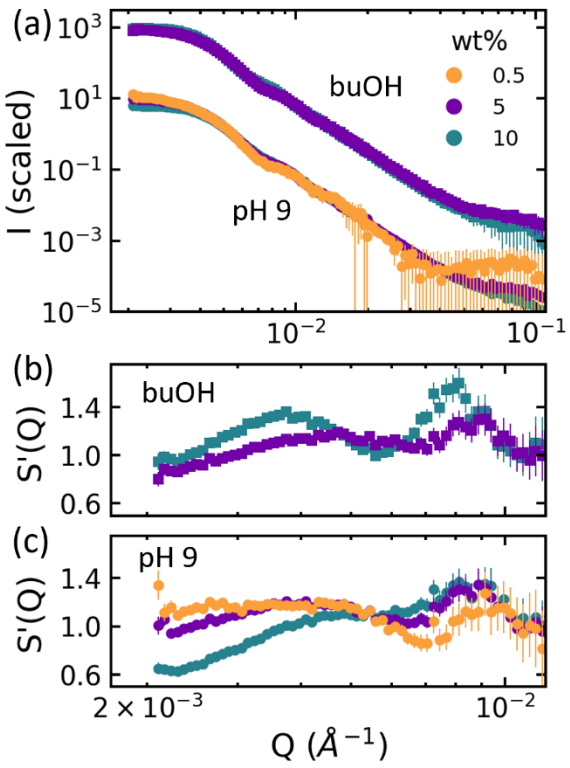

Figure 4: (a) SANS profiles for CS resin in stimuli conditions – with added butanol (top) and at pH 9 (bottom). These were taken at different particle weight percent. The lowest weight percent, 0.5%, does not form a miscible single-phase mixture when butanol is added and is thus excluded from the set. The intensity is normalized for each condition such that the Porod region overlaps, and the conditions are offset by a factor of 100. The intensity is further normalized by the core structure factor to obtain $S'(Q)$, an effective structure factor, which is plotted in (b) and (c).

For the design of paints and coatings, the shear rate dependance of the viscosity is a key consideration as a resin with high low-shear and low high-shear viscosity (i.e., shear thinning) is

desired[29]. In Figure 5, the shear dependance of the viscosity is plotted for different particle weight fractions at different stimuli conditions: low and high pH, and with or without butanol. The samples are Newtonian – the viscosity is independent of the shear rate – at low weight fractions for all stimuli conditions. Some samples with added stimuli exhibit weak shear thinning behavior with a low shear plateau. Strong shear thinning without a low shear plateau is observed for high weight fraction samples at high pH with and without butanol. This shows that pH is much more effective in eliciting the desired rheological response for this resin than the organic solvent. Additionally, since increasing both pH and butanol content further increases the viscosity and shear thinning, the responses arise from independent effects. Although previous studies have investigated pH-responsive and solvent-responsive latex resins, little literature exists that describe independent rheological responses from pH and solvent quality changes.

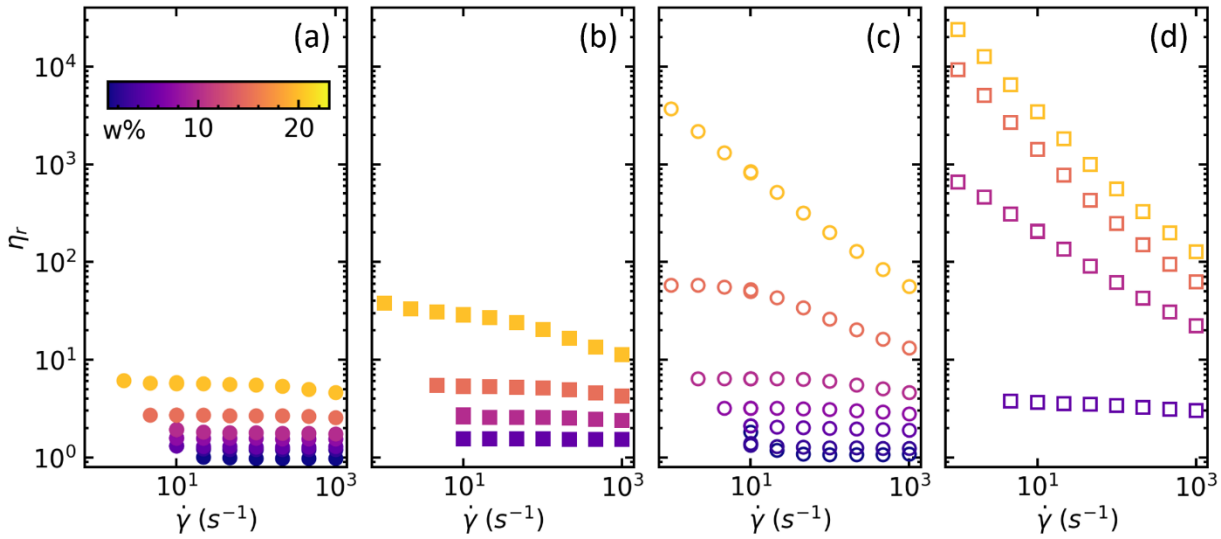

Figure 5: Steady shear rheology of CS resin under different stimuli conditions: (a) ● pH 6, no butanol; (b) ■ pH 6, with butanol; (c) ○ pH 9, no butanol; (d) □ pH 9, with butanol. The samples

with butanol all contain 1:1 mass ratio of butanol to particles. The relative viscosity, η_r, is plotted as a function of shear rate for varying weight fractions from dilute conditions of 1 w% up to a maximum of 20 w%.

The Kreiger-Dougherty equation, $\eta_r = \left(1 - \frac{\phi}{\phi_m}\right)^{-2.5\phi_m}$, is a useful empirical equation to describe the zero-shear viscosity of colloidal suspensions whose behavior can be approximated as effective hard spheres. Where η_r is the relative viscosity, ϕ is the volume fraction of particles, and ϕ_m is the maximum packing fraction for spheres, 0.63. In Figure 6a, the zero-shear viscosity is plotted as a function of the weight fraction of particles for the CS resin at the different stimuli conditions mentioned previously in Figure 5. The data are shifted along the weight fraction axis by a factor, k, such that they overlay the Kreiger-Dougherty equation with the assertion that the volume fraction is $\phi = k \times w$, where w is the weight fraction of particles. This factor is essentially a specific volume of the particles and similar coefficients have been used previously to describe the rheology of swellable colloidal resins.[19] We see in Figure 6b that the data collapse to the Kreiger-Dougherty equation except for the highest concentration samples in high pH conditions. Although the nature of the particle swelling is complex as seen from the structure factor data, the interparticle interactions can be approximated as effective hard sphere interactions. When the particles are swollen at high concentrations, the data no longer follows the Kreiger-Dougherty model so the hard sphere assumption is no longer valid. Under these conditions particle crowding limits free volume, and the specific volume is diminished. The deviation from the hard sphere assumption may arise as the tethered polymers associate and induce an attractive interaction between particles.

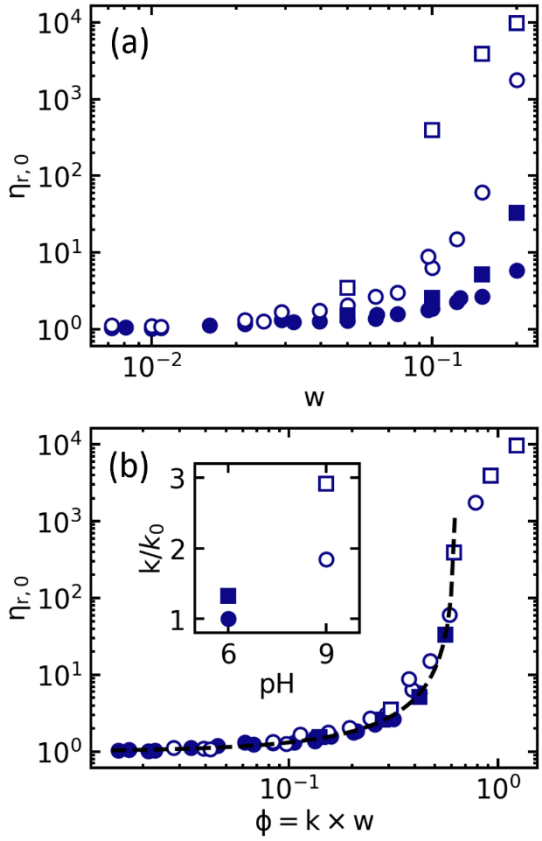

Figure 6: (a) Relative zero shear viscosity of CS resins as a function of weight fraction under different stimuli conditions: ● pH 6, no butanol; ■ pH 6, with butanol; ○ pH 9, no butanol; □ pH 9, with butanol. (b) The weight fractions are shifted by a factor, k, such that the data fall a top the empirical Krieger-Dougherty relation (dotted line), assuming that the volume fraction of particles is $\phi = k \times w$. In the inset of (b) the values of k are normalized to k_0, the value at pH 6 and no butanol. These represent an effective swelling ratio of the particles.

pH-Responsiveness Compared to Literature Resins

We compare the pH-responsiveness of the CS resin to other similar resins presented in literature. The resins that were chosen for comparison consist of polymer-based particles dispersed in water that have an acid or base group that will respond to changes in pH. For a qualitative comparison of the responsiveness, we plot in figure 7 the shear-dependent viscosity normalized by the moles of the acid or base group per gram of particle and by the overall weight fraction of particles. This normalization choice gives more weight to resins that utilize less material for the same rheological response. Here we qualitatively define responsiveness as the overall magnitude of the relative viscosity. Ideally, responsiveness may be defined as a viscosity difference between the maximal and minimal responsive conditions (i.e., when all pH-responsive groups are neutralized and when none are neutralized), however not all references report the rheology of their resin in the latter case. Additionally, while there are several studies in the literature on pH-responsive latex resins, few explicitly show the shear-dependent viscosity of the resin. Each resin has different architectures as depicted schematically in figure 7. The resin investigated in this study was determined to have a core-shell architecture with a crosslinked core and a shell consisting of sparsely grafted, base-responsive, long polymer chains (blue). Tan and coworkers[19] synthesize a resin consisting of an acrylic core and a crosslinked, base-responsive shell (green). Reis and coworkers[20] graft acid-responsive block copolymers to a polystyrene core (orange). Tan and coworkers[18] investigate a single phase, acid-responsive resin (red). The plots shown are under the condition of maximum response for the given resin type. The CS particles in this study show higher overall viscosity per mole of pH-responsive monomer unit used in the polymerization in the window of shear rates which we can directly compare to other resin types. While a direct comparison of the low-shear and high-shear viscosity cannot be made between resin types, we can infer from the mid-shear region that the architecture of the particles in this study illicit a

higher rheological response per mole of responsive group than other resins from literature. This would imply that for the same material input, long polymer tails on particle surfaces may produce more hydrodynamic drag and interparticle interactions than other architectures. This conclusion is qualitative and better methods to compare responsive resins with industrial relevance is necessary. Such methods would require more substantial reporting of shear-dependent viscosity of responsive resins with supporting structural characterizations.

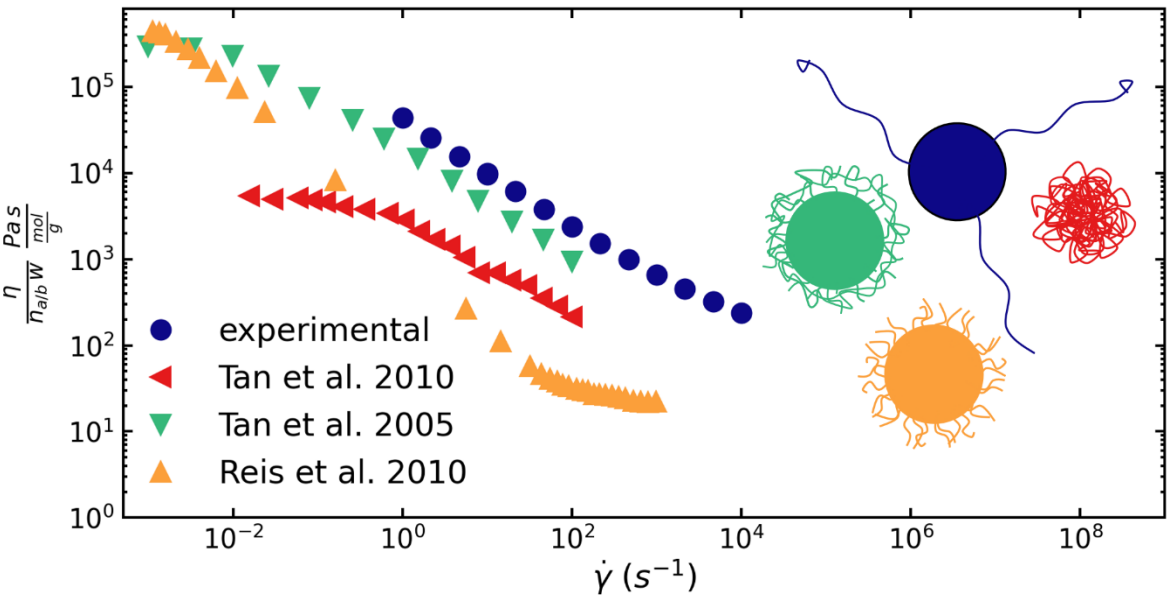

Figure 7: The shear-dependent viscosity of the swollen CS resin at 20 w% (●) is compared to swollen pH responsive resins with different chemistries and architectures from literature. (▼) Polyacrylic core – base-responsive crosslinked shell (▲) Polystyrene core – acid-responsive block copolymer shell (◀) Single phase acid-responsive resin. The viscosities are normalized to the molar number of acid or base units per mass of particle and by the weight fraction of particles. A depiction of each particle architecture is shown in the inset.

The effectiveness of pH swelling of the CS resin plays a crucial role in designing a low VOC paint. The charge repulsion on the resin induces viscosity generation, eliminating the need for solvents that are typically used to swell resins. Additionally, the design and composition of resins impact the location of charge and its effectiveness on inducing desired rheological response. It is important to note that an excessive presence of acid or basic groups in the resin can act as "weak points" for the back-end properties of the paint. As an example, the undesired water absorption can result in weak films with poor performance. By using resins that generate viscosity with less charge, desired application properties can be achieved while minimizing negative impacts on back-end properties. Understanding the architecture of resins with scattering is therefore crucial in providing guidelines for designing resins in low VOC coatings.

ACKNOWLEDGEMENTS

K.J.P. was funded by PPG Industries and by the U.S. Department of Energy, Office of Science, Office of Basic Energy Sciences Energy Frontier Research Centers program under Award No. DE-SC-0022119. A portion of this research used resources at the Spallation Neutron Source, a DOE Office of Science User Facility operated by the Oak Ridge National Laboratory. The beam time was allocated to BL-6, EQ-SANS, on proposal number IPTS-30601.1. A portion of this work made use of the Keck-II facility of Northwestern University’s NUANCE Center, which has received support from the ShyNE Resource (NSF ECCS-2025633), the IIN, and Northwestern’s MRSEC program (NSF DMR-2308691).

REFERENCES

(Word Style “TF_References_Section”).

1. Technical Overview of Volatile Organic Compounds | US EPA. https://www.epa.gov/indoor-air-quality-iaq/technical-overview-volatile-organic-compounds#General%20Definition%20and%20Classifications.

2. Rajaram, S. *CHM049G Global Markets and Advanced Technologies for Paints and Coatings*. (2024).

3. Jiao, C. *et al.* Advances in Waterborne Acrylic Resins: Synthesis Principle, Modification Strategies, and Their Applications. *ACS Omega* **6**, 2443–2449 (2021).

4. Richarz, ; *et al.* Solvents in Water-Borne Coatings. *Industrial and Engineering Chemistry Product Research and Development* **16**, 266–268 (1977).

5. Stockwell, C. E. *et al.* Volatile organic compound emissions from solvent-and water-borne coatings-compositional differences and tracer compound identifications. *Atmos Chem Phys* **21**, 6005–6022 (2021).

6. McCreight, K. W., Stockl, R., Testa, C. & Seo, K. S. Development of low VOC additives to extend the wet edge and open time of aqueous coatings. *Prog Org Coat* **72**, 102–108 (2011).

7. Winnik, M. A. & Feng, J. Latex blends: an approach to zero VOC coatings. *Journal of Coatings Technology* **68**, 39–50 (1996).

8. Kästner, U. The impact of rheological modifiers on water-borne coatings. *Colloids Surf A Physicochem Eng Asp* **183–185**, 805–821 (2001).

9. Lu, C. & Urban, M. W. Stimuli-responsive polymer nano-science: Shape anisotropy, responsiveness, applications. *Prog Polym Sci* **78**, 24–46 (2018).

10. Bhat, B., Pahari, S., Kwon, J. S. Il & Akbulut, M. E. S. Stimuli-responsive viscosity modifiers. *Adv Colloid Interface Sci* **321**, 103025 (2023).

11. Tan, B. H. & Tam, K. C. Review on the dynamics and micro-structure of pH-responsive nano-colloidal systems. *Adv Colloid Interface Sci* **136**, 25–44 (2008).

12. Ballauff, M. Analysis of Polymer Colloids by Small-Angle X-Ray and Neutron Scattering: Contrast Variation. *Adv Eng Mater* **13**, 793–802 (2011).

13. Ballauff, M., Bolze, J., Dingenouts, N., Hickl, P. & Pötschke, D. Small-angle X-ray scattering on latexes. *Macromol Chem Phys* **197**, 3043–3066 (1996).

14. Bolze, J., Hörner, K. D. & Ballauff, M. Small-angle X-ray scattering analysis of the radial structure of latex particles swollen by a nonpolar monomer. *Langmuir* **13**, 2960–2964 (1997).

15. Smith, G. N. *et al.* The internal structure of poly(methyl methacrylate) latexes in nonpolar solvents. *J Colloid Interface Sci* **479**, 234–243 (2016).

16. Quienne, B., Pinaud, J., Robin, J. J. & Caillol, S. From Architectures to Cutting-Edge Properties, the Blooming World of Hydrophobically Modified Ethoxylated Urethanes (HEURs). *Macromolecules* **53**, 6754–6766 (2020).

17. Appell, J., Porte, G. & Rawiso, M. Interactions between nonionic surfactant micelles introduced by a telechelic polymer. A small angle neutron scattering study. *Langmuir* **14**, 4409–4414 (1998).

18. Tan, B. H., Tam, K. C., Dupin, D. & Armes, S. P. Rheological behavior of acid-swellable cationic copolymer latexes. *Langmuir* **26**, 2736–2744 (2010).

19. Tan, B. H., Tam, K. C., Lam, Y. C. & Tan, C. B. Microstructure and rheological properties of pH-responsive core–shell particles. *Polymer (Guildf)* **46**, 10066–10076 (2005).

20. Reis, B. M., Armes, S. P., Fujii, S. & Biggs, S. Characterisation of the dispersion stability of a stimulus responsive core–shell colloidal latex. *Colloids Surf A Physicochem Eng Asp* **353**, 210–215 (2010).

21. Coating processes using waterborne curable film-forming compositions containing polymers derived from natural gas raw materials. (2014).

22. Heller, W. T. *et al.* The suite of small-angle neutron scattering instruments at Oak Ridge National Laboratory. *J Appl Crystallogr* **51**, 242–248 (2018).

23. Heller, W. T. *et al.* drtsans: The data reduction toolkit for small-angle neutron scattering at Oak Ridge National Laboratory. *SoftwareX* **19**, 101101 (2022).

24. Makino, K. & Ohshima, H. Electrophoretic mobility of a colloidal particle with constant surface charge density. *Langmuir* **26**, 18016–18019 (2010).

25. Krieger, I. M. & Dougherty, T. J. A Mechanism for Non-Newtonian Flow in Suspensions of Rigid Spheres. *Transactions of The Society of Rheology* **3**, 137–152 (1959).

26. Guinier, A. & Fournet, G. *Small Angle Scattering*. (Wiley, New York, 1955).

27. Sinha, S. K., Sirota, E. B., Garoff, S. & Stanley, H. B. X-ray and neutron scattering from rough surfaces. *Phys Rev B* **38**, 2297–2311 (1988).

28. Ge, T. & Rubinstein, M. Mobility of Polymer-Tethered Nanoparticles in Unentangled Polymer Melts. *Macromolecules* **52**, 1536–1545 (2019).

29. Larson, R. G., Van Dyk, A. K., Chatterjee, T. & Ginzburg, V. V. Associative thickeners for waterborne paints: Structure, characterization, rheology, and modeling. *Prog Polym Sci* **129**, (2022).